

Journal of Irrigation and Drainage Engineering

Assessing field and laboratory calibration protocols for the Diviner2000 probe in a range of soils with different texture

--Manuscript Draft--

Manuscript Number:	IRENG-7240R2
Full Title:	Assessing field and laboratory calibration protocols for the Diviner2000 probe in a range of soils with different texture
Manuscript Region of Origin:	ITALY
Article Type:	Technical Paper
Manuscript Classifications:	91.10000: Water Resources Planning & Management; 91.14000: Drought management; 91.44000: Ecological aspects; 95: Hydrology/Hydraulics interface Methods (e.g., artificial neural networks, etc.); 97.20000: Irrigation Hydrology; 99: Technology & Applications; 97.23000: Water Balance
Abstract:	<p>Frequency Domain Reflectometry (FDR) down-hole sensors have been increasingly used for soil moisture field monitoring, because they allow measurement, even continuously, along a soil profile; moreover, they can also be installed with a minimal soil disturbance around the access tube.</p> <p>Objectives of the paper were to assess field and laboratory calibration protocols for a FDR capacitance probe (Diviner2000) for a range of soils characterized by different particle size distribution and shrink/swell potential, as well as to propose a practical and effective protocol based on undisturbed soil samples accounting for soil shrinkage/swelling processes characterizing swelling clay soils.</p> <p>Experiments showed that on coarse-textured soils, field calibration under wet, moist and dry conditions, allows estimations of volumetric soil water content with Root Mean Square Error values always lower than 0.058 cm³ cm⁻³. On the contrary, the problems occurring in the field on the finer-textured soils, characterized by a clay content ranging between 36.7% and 45.1% and moderate to high shrink/swell potential, did not permit to identify suitable calibration equations and then accurate estimations of soil water content. For such soils in fact, it was observed a great dispersion of the experimental data and consequently high errors values associated to the site-specific calibration equations, up to 0.121 cm³ cm⁻³ for the soil characterized by the highest clay percentage.</p> <p>The laboratory experiments were carried out by using undisturbed soil monoliths that, compared to sieved soils, have the advantage to account for the natural soil structure surrounding the access tube, as well as to monitor, during sensor calibration experiments, the soil shrinkage processes occurring in clay soils. The Diviner2000 calibration equations obtained in laboratory were characterized by errors values generally lower than those obtained in the field and always smaller than 0.053 cm³ cm⁻³.</p> <p>Finally, in the range of soil water content between about 10% and the maximum observed, the scaled frequency measured by the sensor resulted almost constant at decreasing soil water content. This circumstance can be ascribed to the normal phase of the shrinkage process determining a compensative effects between the reduction of volumetric soil water content and the increasing soil bulk density. The maximum variations of scaled frequency were observed in the range of soil water content for which soil bulk density resulted approximately constant. The knowledge of soil shrinkage characteristic curve assumes therefore a key-role when calibrating FDR sensors on shrinking/swelling clay soils.</p>
Corresponding Author:	Giovanni Rallo, Ph.D. Università di Pisa Pisa, ITALY
Corresponding Author E-Mail:	giovanni.rallo@unipi.it
Order of Authors:	Giuseppe Provenzano, Associate Professor Giovanni Rallo, Ph.D. Hiba Ghazouani, PhD student

1 **Assessing field and laboratory calibration protocols for the Diviner2000 probe in a range of soils**
2 **with different texture**

3 Giuseppe Provenzano¹, Giovanni Rallo^{2*} and Hiba Ghazouani³

4 1) PhD, Associate Professor. Dipartimento Science Agrarie e Forestali, Università degli Studi di Palermo, Viale delle Scienze 12, 90128
5 Palermo, Italy.

6 2) PhD, Researcher. Dipartimento Science Agrarie, Alimentari, Agro-ambientali, Università di Pisa. Via del Borghetto 80, 56124 Pisa,
7 Italy. giovanni.rallo@unipi.it.

8 3) PhD student. Département du Génie des Systemes Horticoles et du Milieu Naturel, Institut Supérieur de Chott Meriém (ISA-CM), BP
9 47, Sousse 4042, Tunisie.

10 *Corresponding author.

11

12 **Abstract**

13 Frequency Domain Reflectometry (FDR) down-hole sensors have been increasingly used for soil
14 moisture field monitoring, because they allow measurement, even continuously, along a soil profile;
15 moreover, they can also be installed with a minimal soil disturbance around the access tube.

16 Objectives of the paper were to assess field and laboratory calibration protocols for a FDR
17 capacitance probe (Diviner2000) for a range of soils characterized by different particle size distribution
18 and shrink/swell potential, as well as to propose a practical and effective protocol based on undisturbed
19 soil samples accounting for soil shrinkage/swelling processes characterizing swelling clay soils.

20 Experiments showed that on coarse-textured soils, field calibration under wet, moist and dry
21 conditions, allows estimations of volumetric soil water content with Root Mean Square Error values
22 always lower than $0.058 \text{ cm}^3 \text{ cm}^{-3}$. On the contrary, the problems occurring in the field on the finer-
23 textured soils, characterized by a clay content ranging between 36.7% and 45.1% and moderate to high
24 shrink/swell potential, did not permit to identify suitable calibration equations and then accurate
25 estimations of soil water content. For such soils in fact, it was observed a great dispersion of the

26 experimental data and consequently high errors values associated to the site-specific calibration
27 equations, up to $0.121 \text{ cm}^3 \text{ cm}^{-3}$ for the soil characterized by the highest clay percentage.

28 The laboratory experiments were carried out by using undisturbed soil monoliths that, compared to
29 sieved soils, have the advantage to account for the natural soil structure surrounding the access tube, as
30 well as to monitor, during sensor calibration experiments, the soil shrinkage processes occurring in clay
31 soils. The Diviner2000 calibration equations obtained in laboratory were characterized by errors values
32 generally lower than those obtained in the field and always smaller than $0.053 \text{ cm}^3 \text{ cm}^{-3}$.

33 Finally, in the range of soil water content between about 10% and the maximum observed, the scaled
34 frequency measured by the sensor resulted almost constant at decreasing soil water content. This
35 circumstance can be ascribed to the normal phase of the shrinkage process determining a compensative
36 effects between the reduction of volumetric soil water content and the increasing soil bulk density. The
37 maximum variations of scaled frequency were observed in the range of soil water content for which
38 soil bulk density resulted approximately constant. The knowledge of soil shrinkage characteristic curve
39 assumes therefore a key-role when calibrating FDR sensors on shrinking/swelling clay soils.

40

41 **Keywords:** Frequency Domain Reflectometry (FDR); Capacitance probe; soil water content; dielectric
42 permittivity; shrinking/swellings soils; calibration protocols.

43

44 **Introduction**

45 During the last decade, Frequency Domain Reflectometry (FDR) sensors have been largely used as
46 equipment for indirect measurements of soil water content (SWC) as they allow, if compared to
47 traditional methods, easy and non-destructive evaluations (Fares and Alva, 2000). Mazahrih et al.
48 (2008) underlined the importance of soil moisture sensors operating in plastic access tubes inserted in
49 the soil (down-hole soil moisture sensor) for eco-hydrological research and/or for precision irrigation

50 scheduling. Compared to other soil moisture sensors, down-hole sensors have the advantage to be
51 installed with a minimal disturbance of the soil around the access tube, being not necessary to excavate
52 any soil pits, as well as to measure SWC along a soil profile. However, the access tubes can be installed
53 only in case of soils with no rocks and/or stones.

54 Among the down-hole FDR sensors, Diviner2000 (Sentek Environmental Technologies, 2001) is a
55 handheld soil water content monitoring device, consisting of a portable display/logger unit connected to
56 an automatic depth-sensing probe in which two electric rings, forming a capacitor, are installed at its
57 extremity. The capacitor and the oscillator represent a circuit generating an oscillating electrical field,
58 that propagates into the soil medium through the wall of the access tube. A schematic view of the
59 probe, for field and laboratory calibration, is shown in fig. 1a,b. The sensor's output is represented by
60 the circuit resonant frequency (raw count), F , depending on the dielectric properties of the soil
61 surrounding the access tube, variable in a range from ~240 to ~330 MHz, which includes the range
62 from ~250 MHz in saturated soil to ~287 MHz in air-dry soil (Evetts et al., 2006). The Enviroscan probe
63 (Sentek Environmental Technologies, 2001) uses the same access tube, but it consists of an array of
64 identical sensors placed permanently at fixed depths and offers the advantage of logging both time and
65 depth series of soil water content.

66

67 **Figure 1**

68

69 It has been demonstrated that 99% of the sensitivity is within a radius of 10 cm from the sensor axes
70 (Paltineanu and Starr, 1997), whereas about half of its sensitivity depends on soil water content in the
71 annular region having thickness ranging between 1 and 2 cm around the surface of the access tube. This
72 last circumstance, however, makes the instruments very sensitive to inconsistencies caused by incorrect
73 installation, resulting in air gaps beside the access tube.

74 The resonant frequency detected by the sensor in the soil (F_s) is scaled to a value SF , ranging
75 between 0 and 1, based on the frequency readings obtained after placing the access tube in air (F_a) and
76 in water (F_w):

$$SF = \frac{F_a - F_s}{F_a - F_w} \quad (1)$$

77

78 The volumetric soil water content, θ [$\text{cm}^3 \text{ cm}^{-3}$] can be then evaluated by solving the calibration
79 equation, which is usually expressed as:

80

$$SF = a \theta^b + c \quad (2)$$

82

83 where a , b and c are fitting parameters. Specifically for Enviroscan, the default equation initially
84 proposed by the manufacturer and derived from an average of three different Australian soils (sands,
85 loams and clay loams), was characterized by $a=0.1957$, $b=0.404$ and $c=0.0285$ and $R^2=0.974$ (Sentek
86 Environmental Technologies, 2001), being θ expressed as a percentage of apparent soil volume.

87 Several Authors stated that the additive constant of eq. (2) can be assumed equal to 0 (Morgan et al.,
88 1999; Geesing et al., 2004; Groves and Rose, 2004; Gabriel et al., 2010); in fact, considering that for θ
89 tending to 0, the corresponding SF values suddenly decrease, for practical applications the related
90 errors can be neglected. The default equation valid for Diviner2000 was obtained under the latter
91 hypothesis, with values of fitting parameters equal to $a=0.2746$, $b=0.3314$ ($R^2=0.9985$). However, the
92 calibration equation proposed by the manufacturer cannot provide accurate measurements of
93 volumetric soil water content for all the soil types, considering that the soil dielectric properties are
94 affected by soil texture and structure. Moreover, agricultural activities also play a significant impact on
95 soil properties like bulk density and organic matter content, so affecting its water storage capacity. Site-

96 specific calibration equations have been therefore largely recommended in order to obtain accurate
97 values of actual volumetric soil water content (Paraskevas et al., 2012; Evett et al., 2006).

98 In the last two decades numerous experiments have been carried out in field and in laboratory to
99 identify site-specific calibration equations for Enviroscan and Diviner2000 sensors on soils
100 characterized by different texture, as well as to evaluate the effects of soil salinity and temperature on
101 the performance of the sensors. Among the first, Mead et al. (1995) presented the calibration and
102 sensitivity analysis of Enviroscan probe to salinity and bulk density changes, related to three soil types
103 (coarse sand, sandy loam with two bulk densities and clay soil). The sensor calibration, carried out
104 under controlled laboratory conditions, showed significant differences even within the two sandy loam
105 soils, which only differed in bulk density. Morgan et al. (1999), using the Enviroscan probe and the
106 default calibration equation on three sandy soil collected in Florida, USA, observed the
107 underestimation of soil water content, when the default calibration equation was used.

108 Alternatively, in shrinking/swelling clay soils, a comparison between Diviner2000 and neutron
109 probe was carried out by Burgess et al. (2006). These Authors indicated that the site-specific
110 calibration equations obtained for both the sensors were substantially different from the default
111 equation even if, after a field calibration the two instruments gave similar estimates of change in soil
112 water content integrated over a meter depth. Even Gabriel et al. (2010), based on field and laboratory
113 measurements with the Enviroscan probe on loamy soils, determined calibration equations
114 characterized by satisfactory coefficients of determination ($R^2=0.96$ and $R^2=0.92$, respectively), whose
115 fitting parameters however resulted significantly different than those characterizing the default
116 equation.

117 Based on experimental data acquired on laboratory columns filled with three different soils (silt loam,
118 loam and clay), Evett et al. (2006) obtained calibration equations for Diviner2000 and Enviroscan
119 characterized by high coefficient of determinations ($R^2>0.99$) and RMSE of the order of $0.02 \text{ cm}^3 \text{ cm}^{-3}$,

120 even if in a previous field calibration of Diviner2000 on two Austrian soils (silty clay loam and silt
121 loam), Evett et al. (2002) presented lower R^2 ($R^2=0.533$ and 0.416) and higher RMSE (RMSE= 0.038
122 and 0.046).

123 According to Paltineanu and Starr (1997), the accuracy of field calibration equation depends on
124 errors related to the sampling of the soil volume investigated by the sensor, that must be done
125 accurately. Moreover, in swelling/shrinking soils, the changes of soil bulk volume with soil water
126 content causes modification in the pore geometry, as indicated by the bulk density-soil water content
127 relationship (soil shrinkage characteristic curve). The coefficient of linear extensibility, *COLE*,
128 (Grossmann et al., 1968; Franzmeier and Ross, 1968), derived by bulk densities of soil clods or
129 undisturbed samples, is generally used for quantifying soil shrink/swell potential. The higher the
130 presence of clay minerals in the smectite group, the greater is the soil shrink/swell potential, whereas
131 illitic clays manifest intermediate shrink/swell potential and kaolinitic clays are least affected by
132 volume changes with soil water content.

133 Malicki et al. (1996) and Davood et al. (2011) suggested that the changes in soil bulk density must
134 not be disregarded when calibrating capacitance sensors. Even Fares et al. (2004), based on field
135 experiments, estimated errors in volumetric soil water content up to 20% when ignoring the variations
136 of soil bulk density.

137 On the contrary, based on laboratory experiments aimed to calibrate the ThetaProbe type ML1
138 (Delta-T Devices, Cambridge, England) on a clay loam soil, Lukanu and Savage (2006) observed a
139 negligible influence of the variations of clay content, soil bulk density and soil temperature detected at
140 different investigation depths, on measured soil water content. Actually, soil bulk density has to be
141 considered a source of uncertainty in volumetric soil water contents estimation, because it influences
142 soil dielectric permittivity (Gardner et al., 1998) and governs the relationship between gravimetric and
143 volumetric soil water contents (Geesing et al., 2004).

144 Hignett and Evett (2008) underlined that the default calibration equation has to be performed in a
145 temperature-controlled room, by using distilled water and homogeneous soil materials (loams or
146 sands), uniformly packed around the sensor. Even if the suggested procedure addressed to a very
147 accurate calibration, the resulting equation cannot be extended to the common field conditions.

148 Despite the manufacturers recommendation to use the default calibration equations to monitor the
149 “relative soil water status”, the need of site-specific calibration arises when actual soil water content is
150 monitored for irrigation scheduling (Evett et al., 2011). The review of Robinson et al. (2008) has
151 recently proposed to consider soil water content as an environmental variable, which should be
152 monitored and shared in common databases aimed to assume a global awareness of the different water-
153 controlled phenomena. With this in mind, the actual values of soil water content have to be considered
154 so that, when using a certain sensor, it is crucial to achieve its highest accuracy.

155 Moreover, the need to standardize methodologies and techniques for laboratory and field
156 calibration of electromagnetic (EM) soil water sensors, has been recently emphasized by Paltineanu
157 (2014) during the Fourth International Symposium on Soil Water Measurement using Capacitance,
158 Impedance and Time Domain Transmission (TDT), hold in Quebec, Canada. Experimental protocols
159 for calibration of any soil water content sensor must provide detailed information describing the
160 sensor’s physical response to the system (operation frequency, response to air and distilled water at ~22
161 °C, room temperature, axial and radial sensitivity of the sensor in distilled water, in air–water and in
162 air–soil interfaces), the soil intrinsic characteristics (texture, clay mineralogy, electrical conductivity,
163 organic matter, gravel content, coefficient of uniformity for bulk density in the soil volume investigated
164 by the sensor). Additionally, the common use of statistical analysis and data interpretation was finally
165 advocated. Even if copious literature exists on FDR sensor calibration for different soils, the lack of a
166 site-specific calibration equation for Sicilian soils in which other researchers are ongoing (Cammalleri
167 et al., 2013; Provenzano et al., 2013; Rallo et al., 2012; Rallo et al., 2014), as well as the requirements

168 of standardizing the calibration protocols, indicated the need to pursue the following objectives: i) to
169 assess field and laboratory protocols to calibrate a Diviner2000 capacitance probe on seven irrigated
170 soils of Western Sicily characterized by a different texture and shrink/swell potential; ii) to analyze
171 their performance and to propose a practical and effective protocol of sensor calibration, based on
172 undisturbed soil samples.

173

174 **Materials and Methods**

175 Experiments were carried out on seven different soils collected in the five irrigated areas of Western
176 Sicily shown in fig. 2, representative of different textural classes. Sampling sites were chosen
177 according to the variability of soil particle distribution and containing limited gravel content, a low
178 salinity and a low amount of organic matter. Only for the site of Castelvetro (CAS), two different
179 locations were investigated: the first (CAS-A) was located in an area characterized by a coarse-textured
180 soil, whereas the second in an area with higher clay content. For the latter, two different soil layers, i.e.
181 0-30 cm and 60-90 cm, were investigated (CAS-B, CAS-C).

182

183 **Figure 2**

184

185 Disturbed soil samples were used for the preliminary particle size analysis as well as to evaluate the
186 gravel content and the soil electrical conductivity. Particle size distribution was determined by coupling
187 a sieving column and the Bouyoucos hydrometer (ASTM 152H). The textural classes were defined
188 according to the USDA classification system (Soil Survey Division Staff, 1993). For each soil sample,
189 the amount of skeleton [g kg^{-1}] was determined by dividing the weight [g] of the material held by a 5
190 mm sieve, to the dry weight [kg] of the original sample from which it was extracted (Pagliai, 1998).

191 The retained material was washed with a Calgon solution (sodium hexametaphosphate), dried in an
192 oven at 105 °C for 48 hours and finally weighted.

193 Soil electrical conductivity, *EC*, was determined on the soil-water extract 1:5 with a conductivity meter
194 (CRISON, microCM 2200) by following the standard procedure presented in Pagliai (1998). For each
195 site, the calibration equation for the Diviner2000 capacitance probe was determined by following the
196 standard field procedure, as suggested in the user's manual, as well as by using a laboratory procedure
197 on undisturbed soil samples, as following described in detail.

198 *Field calibration*

199 Field calibration took place in 2013, during measurement campaigns carried out in three different
200 periods of the year, with the aim to explore a relatively wide domain of soil water contents (wet, moist,
201 dry). The first measurement campaign was generally carried out after significant rainfall events, so that
202 the soil water status was approximately close to the field capacity. The second campaign was
203 accomplished when soil water contents ranged between 0.15 cm³cm⁻³ and 0.25 cm³cm⁻³, while the third
204 was completed at the end of the dry season, for soil water contents lower than about 0.15 cm³cm⁻³.

205 For each selected site, six PVC access tubes (length of 0.35 m) were installed in three groups consisting
206 of two, that were investigated in pairs, during each measurement campaign. To avoid interference, the
207 distance between each group of access tubes was 0.30 m, whereas the distance between the pairs was
208 0.50 m. Access tubes were installed with the specific kit, to reduce the soil disturbance during
209 installation and to ensure the perfect contact between soil and tube, in order to avoid air gaps and
210 preferential water flow.

211 During each measurement campaign, values of scaled frequency (*SF*) were initially acquired by placing
212 the sensor in air and in water and then in both the access tubes, with a 5 cm step, from 5 cm to 25 cm
213 depths. To reduce the measurement errors, scaled frequencies were acquired during the descent and the
214 ascent of the sensor into the tube, and then averaged at each single depth. After the measurements,

215 twelve undisturbed soil samples (8.0 cm diameter and 5.0 cm height), at four distinct soil depths (0-5
216 cm, 5-10 cm, 15-20 cm and 25-30 cm) were collected around each access tube. Immediately after
217 collection, soil samples were leveled, cleaned and weighed (accuracy of balance 0.01 g). Samples were
218 then oven-dried at 105 °C for 48 h, weighted and finally sieved to determine, for each of them, the
219 skeleton content, gravimetric water content, soil bulk volume and finally volumetric water content.
220 Values of soil bulk volume were corrected to accounting for the amount of skeleton identified in the
221 sample, as suggested by Cavazza (2005).

222 ***Laboratory calibration***

223 Laboratory calibration was carried out on undisturbed soil monoliths, having diameter and height equal
224 to about 0.25 m, in which contemporary measurements of scaled frequency (*SF*), gravimetric soil water
225 content (*U*), and the corresponding soil bulk density (ρ_b) were carried out, so to cover the range from
226 field capacity to oven-dry. The dimensions of soil samplers were chosen according to the sensing
227 volume investigated by the sensor, so that about 99% of the sensor response was controlled by the soil
228 inside the monolith.

229 For all the investigated sites, two samples were collected after extensive rainfall events, when soil
230 water content was close to the field capacity, to avoid re-wetting the soil before starting the experiment.

231 The photographic sequence in fig. 3a,i shows the different phases of sampling: soil surface was leveled
232 (fig. 3a) before inserting a 0.30 m long access tube. To ensure verticality, a wood guide and a level
233 were used during installation (fig. 3b,d). Once installed (fig. 3e), the access tube was cleaned inside and
234 the sampler positioned in a way to set the access tube in its axial position (fig. 3f). A hammer was used
235 to gradually tap the sampler in the soil (fig. 3g). Finally, the soil sample was carefully removed (fig.
236 3h,i), wrapped in a plastic film, sealed and transported to the laboratory.

237

238 **Figure 3a,i**

239

240 Scaled frequency and the corresponding weight of the sample were measured during an air-drying
241 process, initially on a daily frequency, which was later reduced according to the water lost.

242 At the same time, the apparent volume of soil monolith was monitored in order to consider the possible
243 shrinking processes characterizing the soils containing swelling clay (Crescimanno and Provenzano,
244 1999). Vertical subsidence of the soil surface was measured on eight marked positions chosen along
245 two orthogonal directions, with a precision Vernier caliper (accuracy 0.1 mm) bolted to a bar, allowing
246 bi-dimensional movements. A micro-switch, glued to the shaft of the caliper, was activated by contact
247 with the soil surface. For each soil water content, the sample height was then obtained by considering
248 the arithmetic mean of the eight values. The sample was then oven-dried and finally its weight and
249 height re-measured. After oven drying, the PVC sampler was removed and the circumference of the
250 core measured, with a flexible tape (accuracy 0.5 mm), at three different heights.

251 The latter measurement allowed to determine the geometrical factor (Bronswijk, 1990), that was
252 assumed valid for the whole shrinking process, which accounts for the relative amount of vertical
253 contraction caused by the change of the sample volume. Based on these measurements it was possible
254 to determine the soil bulk volume corresponding to each measured gravimetric water content, the soil
255 bulk density and finally, the volumetric water content.

256 The knowledge of soil bulk volumes at field capacity, V_{wet} , and after oven-drying, V_{dry} , allowed to
257 quantify the shrink/swell potential of investigated soils according to the coefficient of linear
258 extensibility, $COLE$, evaluated as (Grossman et al., 1968):

259
$$COLE = \left(\frac{V_{wet}}{V_{dry}} \right)^{1/3} - 1 \quad (3)$$

260

261 *Statistical Analysis*

262 The knowledge of volumetric water contents and the corresponding scaled frequencies allowed to fit
263 the calibration equation, represented by the exponential regression of eq. 2, assuming $c=0$. According
264 to Geesing et al., (2004), even though SF is the dependent variable, it was considered as the
265 independent variable, because the equation application is aimed to derive the volumetric water content,
266 θ , from the scaled frequencies SF , provided by the sensor. The exponential regression was obtained on
267 both field and laboratory data, using SYSTAT 13 (Systat, 2014) for nonlinear regression, whose output
268 also provides the coefficient of determination (R^2) and the Root Mean Square Errors (RMSE).

269

270 **Results and Discussion**

271 Figure 4 shows the particle size distributions for the examined soils, indicating the extremely high
272 variability that characterizes them. Tab. 1 summarizes the percentage of clay, silt, sand and soil textural
273 class (Soil Survey Division Staff, 1993), as well as the content of skeleton, the percentage of organic
274 matter (OM) and the values of soil electrical conductivity ($EC_{1:5}$). As can be observed, according to
275 clay and sand contents, whose values ranged respectively from 9.1% to 45.1% and from 17.3% and
276 85.8%, the soils cover different textural classes. According to the percentage of skeleton, variable
277 between 2 e 72 g kg⁻¹, samples can be considered very slightly (<30 g/kg) or slightly stony (30-150
278 g/kg) (Boden, 1994); based on soil electrical conductivity ($EC_{1:5}$), ranged from 0.11 dS m⁻¹ and 0.36 dS
279 m⁻¹, soils can be classified as non-saline (Soil Survey Division Staff, 1993).

280

281 **Figure 4**

282

283 **Table 1**

284

285 ***Field calibration***

286 For the different sites, fig. 5a-g shows the average values of the measured volumetric soil water
287 content, θ , as a function of scaled frequency, SF , measured in the field; the error bars identify the
288 standard deviations of θ , obtained by considering the three undisturbed samples collected at the same
289 depth. Figure 5a-g also illustrates the $\theta(SF)$ relationships suggested by the manufacturer, as well as the
290 experimental regression curves, fitted according to eq. 2, whose coefficients and statistical parameters,
291 indicated in table 2, were obtained assuming the condition of $c=0$, despite the slight regression
292 improvement associated to an intercept different than zero (Paltineanu and Starr, 1997). Table 2 also
293 indicates the ranges of variability of measured soil water contents and RMSE values associated to both
294 the fitting regression curves and the default calibration equation.

295 As can be observed in fig. 5a-g, for the three coarser-textured soils (PAR, CAS-A and MAR),
296 despite the relatively high dispersion of the experimental data, the empirical $\theta(SF)$ relationships
297 obtained in the field resulted very close to the one proposed by the manufacturer, as demonstrated by
298 the similar RMSE values, indicated in table 2. The relatively good performance associated to the
299 default equation ($RMSE \leq 0.08 \text{ cm}^3 \text{ cm}^{-3}$), confirms the general validity of this equation for coarse-
300 textured soils, even if the site-specific calibration equation get to a general improvement of soil water
301 content estimations.

302 On the contrary, for the finer-textured soils (CAS-B, PIN and SAL), it was not possible to
303 determine reliable calibration equations, mainly because of soil cracking observed in the field.

304

305 **Figure 5a-g**

306

307 **Table 2**

308

309 The occurrence of shrinking processes in the finer-textured soils could have determined, even
310 during the second measurement campaign, the opening of cracks in the soil volume investigated by the
311 sensor. This circumstance was particularly evident for the soil PIN, for which the loss of contact
312 between soil and the access tube was visible with the naked eye when the soil was dry, making it
313 impossible to collect any consistent data. For this soil therefore, despite the high R^2 ($R^2=0.87$) and the
314 low RMSE (RMSE=0.042) obtained, considering the limited number of reliable data acquired, the
315 fitted equations cannot be considered appropriate for the whole range of SWCs occurring in the field
316 (fig. 5f).

317 A different problem took place in CAS-C site where, in relation to the investigated soil layer (60-90
318 cm), the variations of soil water content were quite limited, with values of θ that never decreased
319 below 20%. A similar behavior was observed by Fares et al. (2004) on a clay subsoil, in which the
320 minimum soil water content, measured in the field, resulted equal to 18.3%. In this case, it was not
321 possible to identify a calibration equation valid for a wide range of soil water contents (fig. 5e).

322 For the three coarser-textured soils, the default calibration equation generally underestimates the
323 measured volumetric water content when the scaled frequency assumes values lower than about 0.85
324 and overestimate θ in the other cases. Geesing et al. (2004) on a silt-loamy soil and Polyakov et al.
325 (2005) on silty-clay-loam and clay-loam soils observed that the default calibration equation generally
326 overestimates θ . According to the RMSE values associated to the default calibration equations
327 indicated in table 2, it is noteworthy that in finer-textured soils values of RMSE tend to increase at
328 increasing clay content, reaching values even higher than $0.10 \text{ cm}^3 \text{ cm}^{-3}$.

329 Figure 6a-g shows the values of soil bulk density, ρ_b , and gravimetric water content, U , determined
330 on soil cores collected around the access tubes, as a function of sampling depth. As it can be noticed,
331 the average bulk density, increasing at increasing depth in the layer 0-30 cm, is in general characterized
332 by a greater variability in the top-layers compared to the deeper layers; moreover, for each fixed depth,

333 a quite high variability is also evident on gravimetric water content. Even Paltineanu and Starr (1997)
334 underlined the great variability associated to both soil bulk density and gravimetric water content,
335 making it difficult, therefore, to obtain low RMSE values in the field.

336

337 **Figure 6a-g**

338

339 The spatial variability observed on ρ_b and U could be associated to the sampled soil volume, not
340 representative of the fringe volume investigated by the sensor, whereas the temporal variability can be
341 a consequence of the different soil bulk density with soil water content at sampling, associated to the
342 presence of swelling clays.

343 Similar results were found by Paltineanu and Starr (1997) who discussed about the difficulties of
344 getting accurate field measurements of ρ_b and θ in the fringe volume investigated by the sensor,
345 indicating that more accurate calibration equations can be obtained under more controlled laboratory
346 conditions, where it is possible to minimize the uncertainties associated to the field measurements.

347 ***Laboratory calibration***

348 Since the publication of the manufacturer's user manual (Sentek Environmental Technologies,
349 2001), several investigations have been carried out regarding FDR sensors under laboratory conditions.
350 Paltineanu and Starr (1997), Gabriel et al. (2010), Haberland et al. (2014), Rallo and Provenzano,
351 (2014), presented site-specific calibration equations obtained on soil samples prepared in laboratory, by
352 using soils with different texture and sieved through a 5 mm mesh.

353 The laboratory calibration procedure proposed here refers to undisturbed soil monoliths, in order to
354 account for the natural soil structure surrounding the access tube, as well as for the possible variations
355 of apparent soil volume due to the presence of swelling clay. Using such monoliths in fact, allows the
356 contextual monitoring of gravimetric water content, U , soil bulk density, ρ_b , as well as the sensor

357 scaled frequency, SF , during an air-drying process of soil sample. Using undisturbed monolith
358 represents a substantial improvement of field calibration method listed above.

359 For the different examined soils, table 3 shows the maximum gravimetric water content measured
360 immediately after sampling, U_{max} , the minimum and maximum bulk density, $(\rho_{b,min}, \rho_{b,max})$, as well as
361 the coefficient of linear extensibility, $COLE$ and the skeleton content, S . Minimum ρ_b corresponds to
362 the maximum soil water content at sampling, equal approximately to field capacity, whereas maximum
363 ρ_b corresponds to the oven-dry condition. According to the $COLE$ values, investigated soils showed
364 shrink/swell potential ranged from low ($COLE < 0.03$) to high ($0.06 < COLE < 0.09$) (Parker et al., 1977).
365 Similarly to what determined on the smaller samples (8.0 * 5.0 cm), based on the skeleton content, the
366 considered soils are very slightly or slightly stony.

367

368 **Table 3**

369

370 The ratio between the highest and the lowest bulk density, associated to the maximum variations of
371 soil bulk volume, varied from values slightly higher than 1.0 on coarse-textured soils to 1.25, obtained
372 on the sample SAL, containing the highest clay percentages. Moreover, it is noteworthy that this ratio,
373 as well as the $COLE$ values, tend to increase at increasing clay content, confirming the presence of
374 swelling clay in the samples. As known, in fact, a value of the ratio equal to 1.0 is typically associated
375 to rigid soils, whereas higher values are usually obtained on shrinking soils.

376 Figure 7a-g shows, for the different soils, the values θ , SF obtained on both the monoliths and the
377 corresponding fitting regression curves, whose coefficients and statistical parameters (R^2 and RMSE)
378 are indicated in table 4. As can be noticed on fig. 7a-g, a limited dispersion of experimental points
379 around the fitting curve was found only for the finer-textured soils, being practically absent for the
380 others, confirmed by R^2 , higher than 0.84 and RMSE values, always lower than $0.053 \text{ cm}^3 \text{ cm}^{-3}$.

381

382 **Figure 7a-g**

383

384 **Table 4**

385

386 Moreover, for the finer-textured soils and at the highest SF values, significant variations of θ
387 corresponded to limited changes of SF . This circumstance can be ascribed to the effects of increasing
388 bulk density, observed at decreasing water content, on the soil dielectric permittivity; in fact, mainly
389 during the initial phase of the drying process, any reduction of soil porosity changes the mutual
390 proportions of water, air and solid particles, so affecting the soil dielectric permittivity and
391 consequently the resonant frequency, F_s , detected by the sensor. As observed by Davood et al. (2012),
392 for a fixed water content, there exists a positive linear relationship between soil dielectric permittivity
393 and soil bulk density, as a consequence of the higher mass of solid particles per unit soil volume. In
394 other terms, the almost constant SF values depend on the combined effect between the reduction of soil
395 water content and the contextual increase of soil dielectric permittivity. Other possible explanations for
396 this behavior were provided by Evett. et al. (2008), who referred how capacitance sensors are
397 influenced by some properties of the soil–water system around the access tube and not only by the
398 water content. Such properties have been related to the soil structure and to the non uniform penetration
399 in the soil of the electromagnetic field generated by the sensor (Evett and Steiner, 1995), as well as to
400 the distortion of the electromagnetic field generated by the individual arrangement of soil peds and by
401 the pattern of water content in the peds around the access tube.

402 In order to exclude the effects of variations of bulk density on volumetric soil water content, SF
403 values were then represented as a function of the gravimetric water content, U , rather than θ . For the
404 different soils, fig. 8a-g shows, as a function of U , the values of scaled frequency, SF (main axes) and

405 of soil bulk density, ρ_b (secondary axes), obtained on both the monoliths. As known, the relationship
406 $\rho_b(U)$ represents the soil shrinkage characteristic curve.

407

408 **Figure 8a-g**

409

410 By observing fig.8a-g, it can be noticed that the values of soil bulk density resulted quite different
411 between the soils, which particularly manifested a quite dissimilar behavior and exhibited, in several
412 cases, extensive variations of ρ_b in the range of investigated U , as a consequence of the shrinking
413 processes occurred in the samples.

414 Except that for the coarse-textured soils (PAR, CAS-A and MAR) characterized by the absence or
415 limited soil shrinkage ($COLE < 0.03$), for the other samples very limited variations of SF occurred in the
416 range of gravimetric soil water contents higher than a certain threshold value ($U^* \approx 0.10 \text{ g g}^{-1}$). This
417 threshold represents roughly the lower limit of the normal phase of the shrinking process, in which the
418 variations of soil bulk volume are approximately proportional to the gravimetric water content U . For
419 gravimetric water content smaller than the threshold, it can be noticed that the variations of soil bulk
420 density are limited or absent (residual phase of soil shrinkage characteristic curve) and, at the same
421 time, the most significant variations of sensor scaled frequency occur.

422 Similarly to what observed on the $\theta(SF)$ experimental data pairs for finer-textured soils, even the
423 $SF(U)$ data showed analogous behavior, considering that only in correspondence of the residual phase
424 of the shrinking process ($U < U^*$; $\rho_b = \text{constant}$), SF values tend rapidly to increase at rising U ;
425 otherwise, variations of SF tend gradually to reduce at increasing U , during the normal phase of the
426 shrinkage process ($U > U^*$ and $\rho_b = f(U)$), up to be absent at the highest water contents.

427 Soil contraction, in fact, determines changes in bulk soil permittivity, ε_b , depending on the rates of
428 water, air and solid matrix in the fringe volume investigated by the sensor. At the beginning of

429 shrinkage process, the relatively small reduction of SF at decreasing U can be attributed to the
430 circumstance that the variations in water content are in whole or in part compensated by the changes of
431 soil bulk density. In other words, as shown by Gong et al. (2003) and more recently by Davood et al.
432 (2012), this behavior is caused by the increase of the solid particles per unit of soil volume and
433 consequently by the higher contribution of the soil permittivity, since the solid particles are
434 characterized by values of dielectric constant higher than the air.

435

436 **Conclusions**

437 In this paper, field and laboratory calibration equations for Diviner2000 capacitance probe were
438 assessed and a practical and effective protocol for sensor calibration proposed. Experiments considered
439 seven Sicilian irrigated soils characterized by different textures classes and shrink/swell potential, quite
440 limited content of skeleton, as well as low values of soil electric conductivity.

441 The results of field calibration, carried out by using the procedure suggested by the manufacturer
442 under wet, moist, and dry conditions, indicated that for the three coarser-textured soils the default
443 calibration equation can be considered valid, resulting in RMSE values associated to estimated
444 volumetric soil water content, θ , always lower than $0.080 \text{ cm}^3 \text{ cm}^{-3}$. However, for these soils the site-
445 specific calibration equation improved the estimation of θ , as confirmed by the systematic reduction of
446 RMSE to values always lower than $0.058 \text{ cm}^3 \text{ cm}^{-3}$.

447 For the finer-textured soils, instead, some problems occurred in the field during the sensor
448 calibration, because of the presence of swelling clays, making the field calibration not reliable for these
449 soils. In fact, soil shrinkage processes occurring under the driest examined condition and visibly
450 evident for the soil PIN, determined the opening of cracks and the presence of air gaps in the fringe
451 volume investigated by the sensor. The loss of contact between soil and access tube, made it impossible
452 to collect any consistent data to be used for sensor calibration. Otherwise, in the site CAS-C, due the

453 investigated soil depth (60-90 cm), it was possible to explore only a limited range of soil water
454 contents, between about 0.20 and 0.30 cm³ cm⁻³. For finer-textured soils, RMSE values associated to
455 the site-specific calibration equation resulted generally high, with values up to 0.121 cm³ cm⁻³ for the
456 site SAL, characterized by the highest clay percentage. The great dispersion of $\theta(SF)$ data pairs not
457 only resulted as a consequence of changes in soil water content, but also from the observed spatial and
458 temporal variability of soil bulk density in the fringe volume investigated by the sensor. In line with
459 Paltineanu and Starr (1997) therefore, more controlled laboratory conditions for sensor calibration
460 allow minimizing the recognized uncertainties associated to the field measurements. Moreover,
461 compared to tedious and time-consuming field calibration procedure, in laboratory it is possible to
462 explore with continuity a wide range of soil water contents.

463 Laboratory calibration was carried out on undisturbed soil monoliths that, compared to the
464 traditionally considered sieved samples, have the advantage to account for the natural soil structure. For
465 shrinking/swelling clay soils, using undisturbed soil monoliths allows to monitor the increasing bulk
466 density at decreasing soil water content and to limit the presence of air gaps between the access tube
467 and the surrounding soil, as occurred in the field.

468 For the considered soils it was observed that the ratio between the highest and the lowest bulk
469 density, corresponding respectively to the oven dry condition and to maximum water content, resulted
470 ranging between 1.0, measured on the rigid sandy-loam soil (PAR) and 1.25, obtained on the shrinking
471 clay soil (SAL), with values basically increasing at increasing clay content. With the laboratory
472 calibration protocol, compared to the field procedure, it was possible to limit the dispersion of the
473 experimental $\theta(SF)$ values around the fitting curve, as confirmed by the general reductions of the
474 corresponding RMSE, whose values never exceeded 0.030 cm³ cm⁻³ for coarse-textured soils and 0.053
475 cm³ cm⁻³ for fine-textured soils. For the latter, it was also observed that at the highest SF , significant
476 variations of θ were associated to limited changes in the scaled frequency, as a consequence of the

477 effects of shrinkage processes on soil dielectric permittivity and then on resonant frequency detected by
478 the sensor, confirming that capacitance sensors are influenced by properties of the soil–water system
479 around the access tube and not only by the changes in soil water content.

480 In order to exclude the effects of soil bulk density on soil water content, it was suggested to
481 represent the sensor scaled frequency as a function of gravimetric water content, U , rather than
482 volumetric θ , thus to investigate, at the same time, even on the consequences of soil shrinkage
483 processes on SF .

484 Experimental results showed that the values of SF rapidly increased at increasing U in
485 correspondence with the residual phase of the shrinking process (constant bulk density), to become
486 approximately constant during the normal phase of the shrinking process, in which bulk density is a
487 function of soil water content. In other terms, at relatively high U , it was observed that the variations in
488 soil water content were in whole or in part compensated by the changes of soil bulk density, so that the
489 final scaled frequency measured by the sensor resulted approximately constant.

490 When calibrating FDR sensors on shrinking/swelling clay soils, is then necessary to determine the
491 soil shrinkage characteristic curve whose knowledge, associated to the sensor calibration equation,
492 expressed as $U(SF)$, allows to determine the volumetric water content.

493 Further investigations are however necessary to identify how the soil shrinkage characteristic curve
494 can be introduced in the sensor calibration equation in terms of $\theta(SF)$, as well as to verify the
495 possibility of indirect estimation of the calibration equation parameters based on easy-to-measure soil
496 physical variables.

497

498 **Acknowledgements**

499 The research was co-financed from Ministero dell'Istruzione, dell'Università e della Ricerca
500 (www.miur.it) under the project PRIN 2010-2011 and Università degli Studi di Palermo, under the
501 project FFR 2012, both coordinated by G. Provenzano.

502 The contribution to the manuscript has to be shared between authors as following: Experimental
503 set-up, data processing and final revision of the text have to be divided equally between Authors. Field
504 data collection was cared by G. Rallo. Text was written by G. Rallo and G. Provenzano.

505

506

507 **References**

508 Boden, A.G. 1994. *Bodenkundliche Kartieranleitung*, E. Schweizerbart'sche Verlagsbuchhandlung,
509 Stuttgart.

510 Bronswijk, J.J.B. 1990. Shrinkage geometry of a heavy clay soil at various stresses, *Soil Science*
511 *Society of America Journal*, 54:1500–1502.

512 Burgess, P.J., Reinhard, B.R., Pasturel, P. 2006. Compatible measurements of volumetric soil water
513 content using a neutron probe and Diviner 2000 after field calibration. *Soil Use and Management*,
514 22:401–404.

515 Cavazza, L. 2005. *Terreno agrario: Il comportamento fisico*. Reda Editore (in Italian).

516 Cammalleri C., Rallo G., Agnese C., Ciraolo G., Minacapilli M., and Provenzano, G. (2013).
517 Combined use of eddy covariance and sap flow techniques for partition of ET fluxes and water
518 stress assessment in an irrigated olive orchard. *Agricultural Water Management*, 120:89-97. DOI:
519 10.1016/j.agwat.2012.10.003.

520 Crescimanno, G., Provenzano, G. 1999. Soil shrinkage characteristic in clay soils: measurement and
521 prediction. *Soil Science Society of America Journal*, 63:25-32.

522 Davood, N.K., Shorafa, M., Heidari, A. 2012. Estimating Soil Water Content from Permittivity for
523 Different Mineralogies and Bulk Densities. *Soil Science Society of America Journal*, 76:1149–
524 1158.

525 Evett, S.R., Heng, L.K., Moutonnet, P., Nguyen, M.L. 2008. Field estimation of soil water content: A
526 practical guide to methods, instrumentation, and sensor technology. In: S.R. Evett, L.K. Heng, P.
527 Moutonnet, and M.L. Nguyen (eds.). IAEA-TCS-30. Intl. Atomic Energy Agency, Vienna, Austria,
528 123–129.

529 Evett, S. R., Ruthardt, B., Kottkamp, S., Howell, T., Scheneider, A., Tolk, J. 2002. Accuracy an
530 precision of soil water measurements by neutron, capacitance and TDR methods, in: *Proceedings of*
531 *the 17th Water Conservation Soil Society Symposium, Thailand*.

532 Evett, S.R., Schwartz, R.C., Mazahreh, N., Jitan, M., Shaqir, I.M. 2011. Soil water sensors for
533 irrigation scheduling: Can they deliver a management allowed depletion? *Acta Horticulturae, Proc.*
534 *International Symp. Olive Irrig. and Oil Quality, Nazareth, Israel, 6-10 December 2009*, 888:231-
535 237.

536 Evett, S.R., Steiner, J.L. 1995. Precision of neutron scattering and capacitance type soil water content
537 gauges from field calibration. *Soil Science Society of America Journal*, 59:961-968.

538 Evett, S.R., Tolk, J.A., Howell, T.A. 2006. Soil profile water content determination: Sensor accuracy,
539 axil response, calibration, temperature dependence, and precision. *Vadose Zone Journal*, 5:894–
540 907.

541 Fares, A., Alva, A.K. 2000. Evaluation of capacitance probes for optimal irrigation of citrus through
542 soil moisture monitoring in an Entisol profile. *Irrigation Science*, 19:57-64.

543 Fares, A., Buss, P., Dalton, M., El-Kadi, A.I., Parsons, L.R. 2004. Dual field calibration of capacitance

544 and neutron sensors in a shrinking-swelling clay soil. *Vadose Zone Journal*, 3:1390–1399.

545 Franzmeier, D. P., Ross, S. J. 1968. Soil swelling: laboratory measurement and relation to other soil
546 properties. *Soil Sci. Soc. Am. Proc.*32:573-577.

547 Gabriel, J.L., Lizaso, J.I., Quemada, M. 2010. Laboratory versus field calibration of capacitance
548 probes. *Soil Science Society of America Journal*, 74:593-601.

549 Gardner, C.M.K., Dean, T.J., Cooper, J.D. 1998. Soil water content measurement with a high-
550 frequency capacitance sensor. *Journal of Agricultural Engineering Research*, 71:395-403.

551 Geesing, D., Bachmaier, M., Schmidhalter, U. 2004. Field calibration of a capacitance soil water probe
552 in heterogeneous fields. *Australian Journal of Soil Research*, 42:289-299.

553 Gong, Y. S., Cao, Q.H., Sun, Z.J. 2003. The effects of soil bulk density, clay content and temperature
554 on soil water measurement using time domain reflectometry. *Hydrological Processes*. 17:3601-
555 3614.

556 Grossman, R. B., Brasher, B. R., Franzmeier, D. P., Walker, J.L. 1968. Linear extensibility as
557 calculated from natural-clod bulk density measurements. *Soil Science Society of America*
558 *Proceedings*. 32, 570-573.

559 Groves, S.J., Rose, S.C. 2004. Calibration equations for Diviner 2000 capacitance measurements of
560 volumetric soil water content of six soils. *Soil Use and Management*, 20:96–97.

561 Haberland, J., Gálvez, R., Kremer, C., Carter, C. 2014. Laboratory and Field Calibration of the Diviner
562 2000 Probe in Two Types of Soil. Published online on *Journal of Irrigation and Drainage*
563 *Engineering*. DOI:10.1061/(ASCE)IR.1943-4774.0000687.

564 Hignett, C., Evett, S. 2008. Direct and Surrogate Measures of Soil Water Content. In: Evett, S.R., L.K.
565 Heng, P. Moutonnet, and M.L. Nguyen, editors. *Field Estimation of Soil Water Content: A*
566 *Practical Guide to Methods, Instrumentation, and Sensor Technology*. IAEA-TCS-30. International
567 Atomic Energy Agency, Vienna, Austria. ISSN 1018-5518.

568 Lukanu, G., Savage, M.J. 2006. Calibration of a frequency-domain reflectometer for determining soil-
569 water content in a clay loam soil. *Water SA*, Vol. 32(1).

570 Malicki, M.A., Plagge, R., Roth, C.H. 1996. Improving the calibration of dielectric TDR soil moisture
571 determination taking into account the solid soil. *European Journal of Soil Science*, 147(3):357–366.

572 Mazahrih, N.Th., Katbeh-Bader, N., Evett, S.R., Ayars, J.E., Trout, T.J. 2008. Field Calibration
573 Accuracy and Utility of Four Down-Hole Water Content Sensors. *Vadose Zone Journal*, 7:992.

574 Mead, R.M., Ayars, J.E., Liu J. 1995. Evaluating the influence of soil texture, bulk density and soil
575 water salinity on a capacitance probe calibration. *ASAE Paper*, 95-3264.

576 Morgan, K.T., Parsons, L.R., Wheaton, T.A., Pitts, D.J., Obreza, T.A. 1999. Field calibration of a
577 capacitance water content probe in fine sand soils. *Soil Science Society of America Journal*, 63, 987-
578 989.

579 Pagliai, M. 1998. *Metodi di analisi fisica del suolo*. Editore Franco Angeli (in Italian). ISBN:
580 9788846404268.

581 Paltineanu, I.C., Starr, J.L. 1997. Real-time soil water dynamics using multisensor capacitance probes:
582 laboratory calibration. *Soil Science Society of America Journal*, 61:1576–1585.

583 Paltineanu, I.C. 2014. On the importance of international standardization of methodologies and
584 techniques for laboratory and field calibration of soil water measurement sensors based on
585 capacitance, impedance, and TDT. *Transactions of the fourth international symposium on soil
586 water measurement using capacitance, impedance and time domain transmission*. Montreal,
587 Quebec, Canada. July, 16–18. ISBN 10:0982796935; ISBN 13: 978-0-9827969-3-1.

588 Paraskevas, C., Georgiou, P., Ilias, A., Panoras, A., Babajimopoulos, C. 2012. Calibration equations for
589 two capacitance water content probes in a lysimeter field. *International Agrophysics*, 26:285-293.

590 Parker, J.C., Amos D.F., Kaster, D.L. 1977. An evaluation of several methods of estimating soil
591 volume change. *Soil Science Society of America Journal*, 41:1059-1064.

592 Polyakov, V., Fares, A., Ryder, M.H. 2005. Calibration of a capacitance system for measuring water
593 content of tropical soil. *Vadose Zone Journal*, 4:1004-1010.

594 Provenzano, G., Tarquis, A. M., Rodriguez-Sinobas, L. 2013. Soil and irrigation sustainability
595 practices. *Agricultural Water Management*, 120(31): 1-4.

596 Rallo G., Agnese C., Minacapilli M., Provenzano G. 2012. Comparison of SWAP and FAO Agro-
597 Hydrological Models to Schedule Irrigation of Wine Grape. *J. Irrig. Drain Eng.*, 138(7), 581–591.
598 DOI: 10.1061/(ASCE)IR.1943-4774.0000435.

599 Rallo G., Baiamonte G., Manzano Juárez J. and Provenzano G. 2014. Improvement of FAO-56 Model
600 to Estimate Transpiration Fluxes of Drought Tolerant Crops under Soil Water Deficit: Application
601 for Olive Groves. *Journal of Irrigation and Drainage Engineering*, 140(9).
602 DOI:10.1061/(ASCE)IR.1943-4774.0000693.

603 Rallo, G., Provenzano, G. 2014. Discussion of “Laboratory and field calibration of the Diviner2000
604 probe in two types of soil” by J. Haberland, PhD, R. Galvez, C. Kremer, PhD, and C. Carter.
605 DOI:10.1061/(ASCE)IR.1943-4774.0000856, 07014063.

606 Robinson, D.A., Campbell, C.S., Hopmans, J.W., Hornbuckle, B.K., Jones, S.B., Knight, R., Ogden, F.,
607 Selker, J., Wendroth, O. 2008. Soil moisture measurement for ecological and hydrological
608 watershed-scale observatories: A review. *Vadose Zone Journal*, 7:358–389.

609 Sentek Environmental Technologies. 2001. Calibration of the Sentek Pty Ltd Soil Moisture Sensors.
610 Sentek Pty Ltd, Stepney, South Australia, 60.

611 Soil Survey Division Staff. 1993. Soil survey manual. Soil Conservation Service. U.S. Department of
612 Agriculture Handbook 18.

613 SYSTAT. 2014. Systat for Windows: Statistics. Ver. 13. Systat, Evanston, IL.

614

615

616
617
618
619
620
621
622
623
624
625
626
627
628
629

Figure Caption List

- Figure 1a,b – Schematic view of Diviner2000 probe; a) field calibration, b) laboratory calibration**
- Figure 2 - Map and localization of investigated sites (from Google Earth)**
- Figure 3a,i – Steps for collecting undisturbed soil monoliths**
- Figure 4 – Particle size distribution obtained on the investigated soils**
- Figure 5a-g - θ , SF data pairs measured in the field on different soils, in three experimental measurement campaigns. Error bars indicate the standard deviations of measured θ . Fitting regressions, as well as the default calibration equation are also shown**
- Figure 6a-g - Values of soil bulk density (black dots) and corresponding gravimetric water contents (white dots) measured on undisturbed soil samples (8.0 * 5.0 cm) as a function of soil depths**
- Figure 7a-g - Values θ (SF) measured on undisturbed soil monoliths and related fitting equation**
- Figure 8a-g - SF(U) (white dots) and ρ_b (U) (black dots) measured on undisturbed soil monoliths**

Tab. 1 –Physical properties of investigated soils

Site	ID	Clay [%]	Silt [%]	Sand [%]	Soil textural class (USDA)	Skeleton [g kg⁻¹]	OM [%]	EC_{1:5} [dS m⁻¹]
Partinico	PAR	9.1	5.1	85.8	S-L	20	n.d.	0.11
Castelvetrano	CAS-A	20.0	16.3	63.7	L-S-C	17	2.0	0.31
Marsala	MAR	24.6	26.9	48.5	L-S-C	32	2.6	0.22
Castelvetrano	CAS-B	38.7	13.4	42.4	L-C	4	1.9	0.18
Pietranera	PIN	37.4	33.8	28.8	L-C	32	2.0	0.35
Castelvetrano	CAS-C	36.7	17.9	45.3	S-C	2	2.0	0.18
Salemi	SAL	45.1	37.6	17.3	C	72	2.0	0.23

Tab- 2 –RMSE associated to the fitting regressions and default calibration equations. The number of measurements, the range of θ and the parameters of eq. 3 are also indicated for the different soils.

ID	N	Range of θ [cm ³ cm ⁻³]		Fitting regression equation				Default equation
		min	max	<i>a</i>	<i>b</i>	R ²	RMSE	RMSE [cm ³ cm ⁻³]
PAR	24	0.01	0.37	0.439	2.869	0.84	0.049	0.054
CAS-A	24	0.03	0.30	0.359	2.130	0.76	0.054	0.080
MAR	18	0.08	0.29	0.482	2.650	0.73	0.058	0.063
CAS-B	24	0.05	0.33	0.473	1.709	0.67	0.074	0.100
PIN	16	0.17	0.49	0.453	0.446	0.87	0.042	0.166
CAS-C	27	0.20	0.31	0.347	1.084	0.35	0.040	0.110
SAL	24	0.04	0.33	0.576	2.007	0.49	0.121	0.113

Tab. 3 - Values of maximum gravimetric water content (U_{max}), minimum ($\rho_{b,min}$) and maximum ($\rho_{b,max}$) soil bulk density, coefficient of linear extensibility (COLE) and skeleton content, S , measured on undisturbed soil monoliths

ID	U_{max} [g g ⁻¹]	$\rho_{b,min}$ [g cm ⁻³]	$\rho_{b,max}$ [g cm ⁻³]	$\frac{\rho_{b,max}}{\rho_{b,min}}$ [-]	COLE [-]	S [g kg ⁻¹]
PAR	0.28	1.50	1.51	1.00	0.000	20
CAS_A	0.27	1.40	1.49	1.06	0.020	21
MAR	0.29	1.31	1.33	1.01	0.003	32
CAS_B	0.17	1.57	1.74	1.11	0.035	4
PIN	0.21	1.40	1.70	1.21	0.066	10
CAS_C	0.20	1.41	1.65	1.17	0.054	3
SAL	0.24	1.32	1.65	1.25	0.077	72

Tab. 4 - Coefficients a and b of eq. 3 and related R^2 and RMSE, obtained on undisturbed monoliths. The total number of experimental determinations, N , on both the samples is also indicated

ID	N	a	b	R^2	RMSE [cm³ cm⁻³]
PAR	38	0.607	5.013	0.94	0.029
CAS_A	45	0.571	5.813	0.93	0.015
MAR	52	0.555	5.127	0.95	0.030
CAS_B	29	0.393	6.590	0.95	0.039
PIN	16	0.282	5.152	0.94	0.044
CAS_C	30	0.534	7.310	0.87	0.053
SAL	59	0.587	10.493	0.84	0.049

Fig1

[Click here to download Figure: fig1.pdf](#)

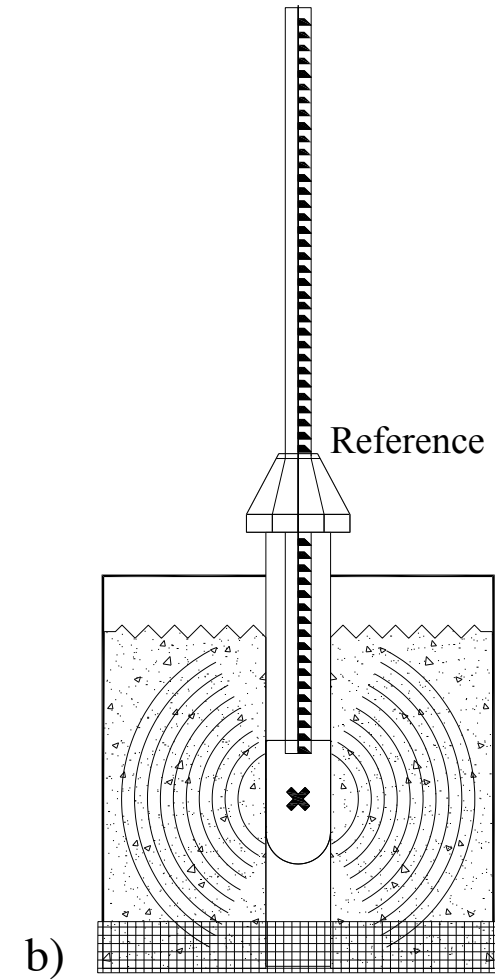
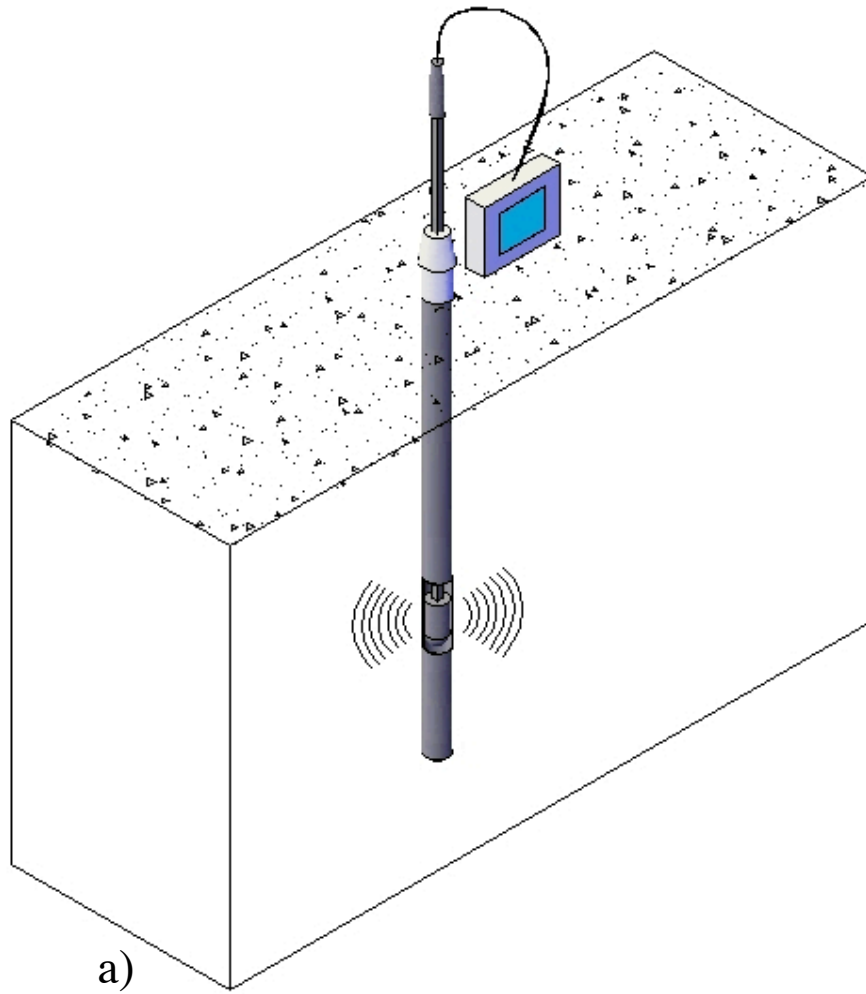
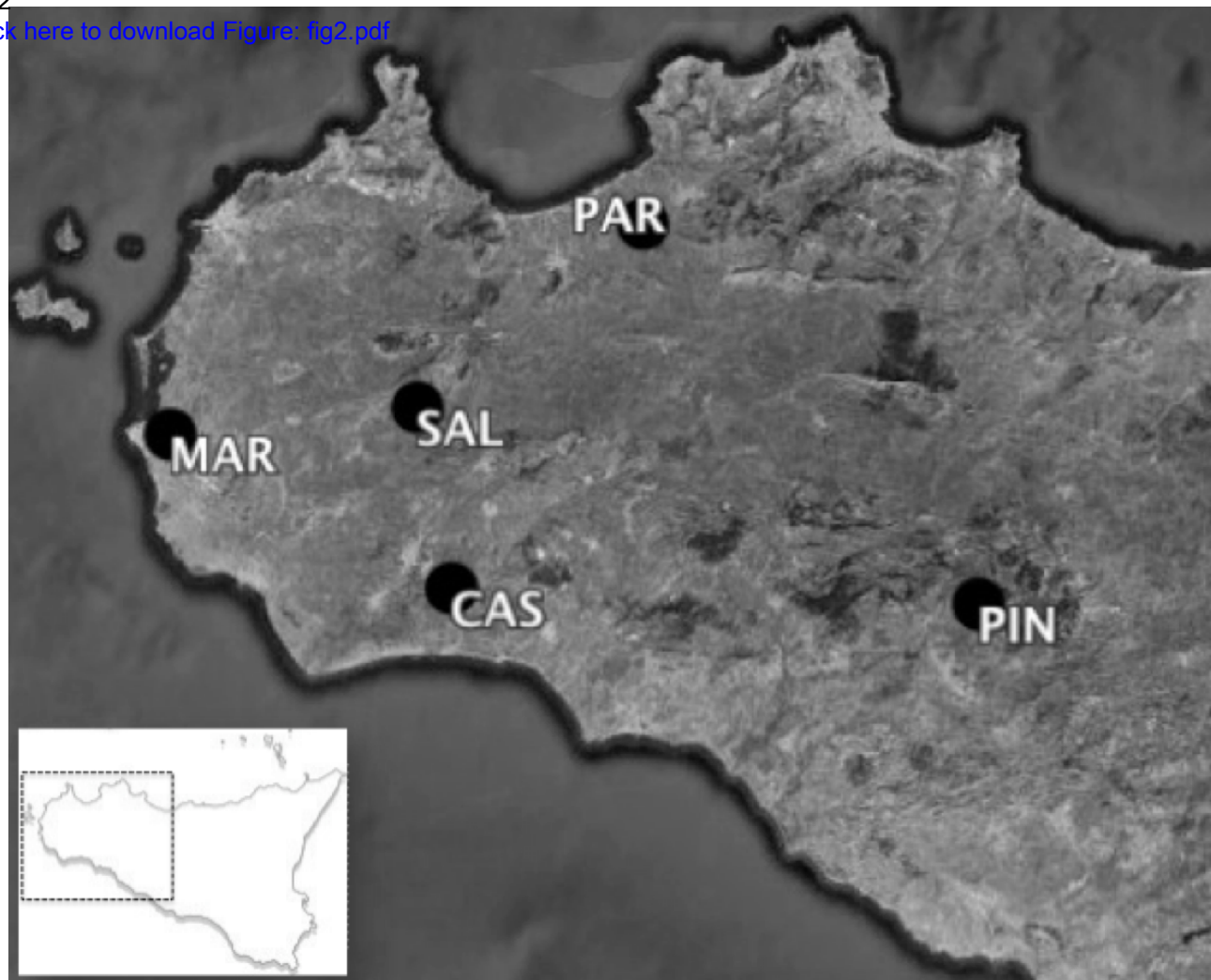


Fig2

[Click here to download Figure: fig2.pdf](#)



Site	ID	UTM ED50 coordinates [m]	
		East	North
Partinico (PA)	PAR	330516.8	4208994.2
Castelvetrano (TP)	CAS	310086.4	4168408.9
Marsala (TP)	MAR	278561.3	4186111.9
Pietranera (AG)	PIN	367878.4	4165752.0
Salemi (TP)	SAL	305920.6	4188651.2

Fig3

[Click here to download Figure: fig3.pdf](#)

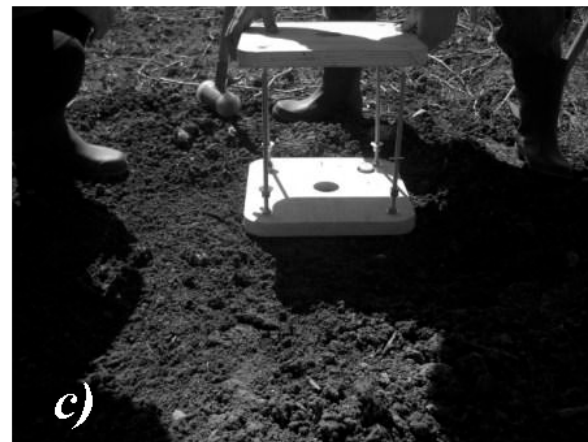
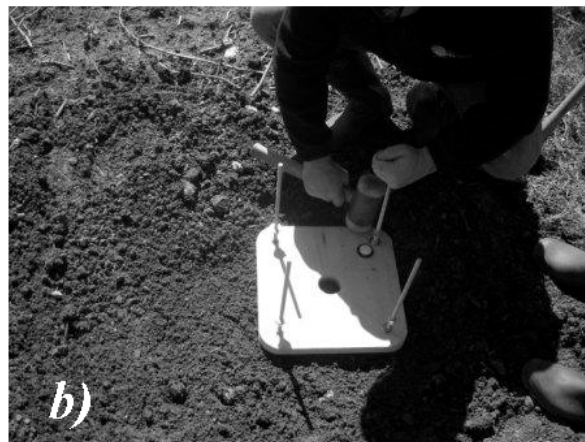


Fig4
[Click here to download Figure: fig4.pdf](#)

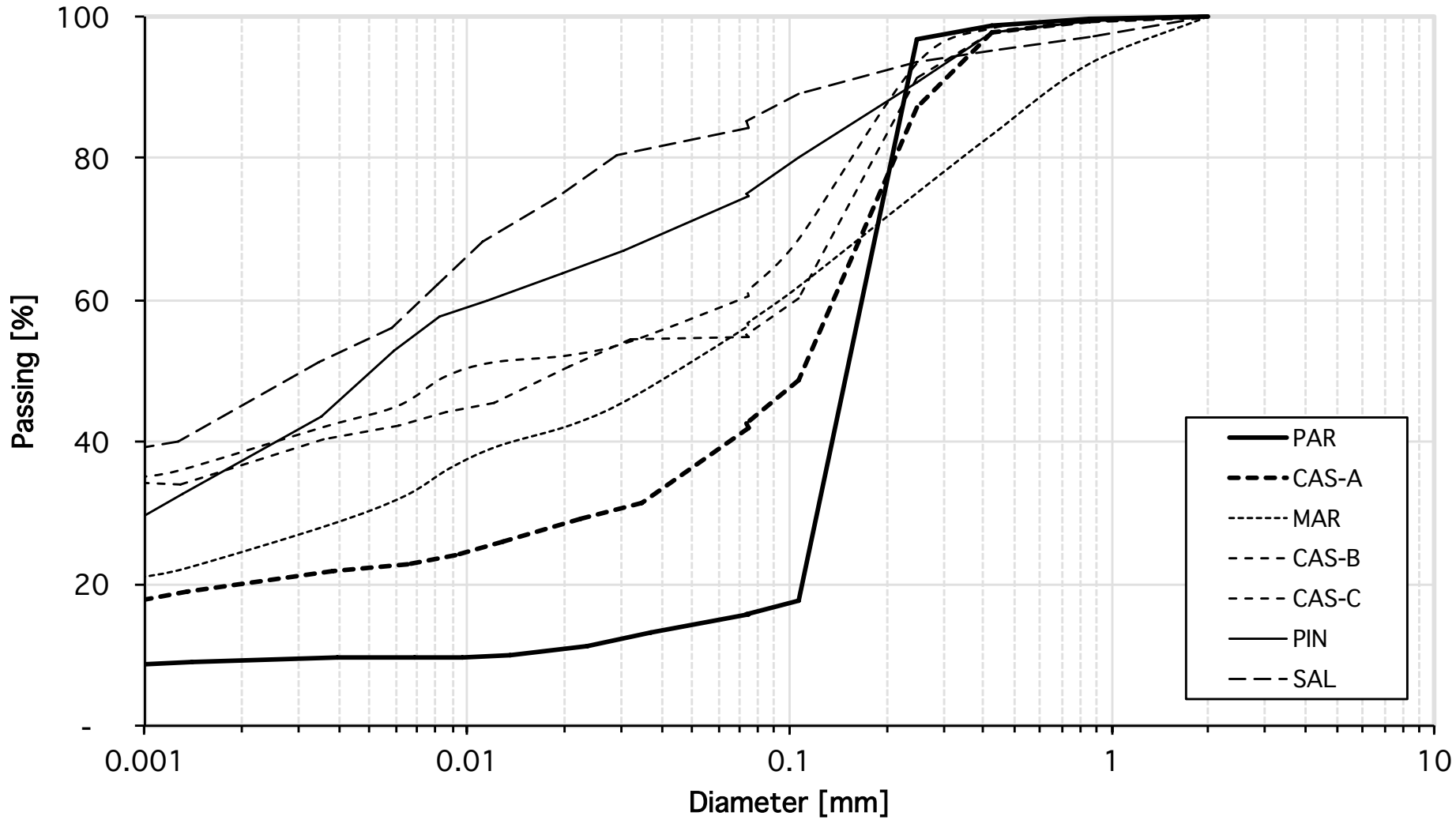


Fig5
[Click here to download Figure: fig5.pdf](#)

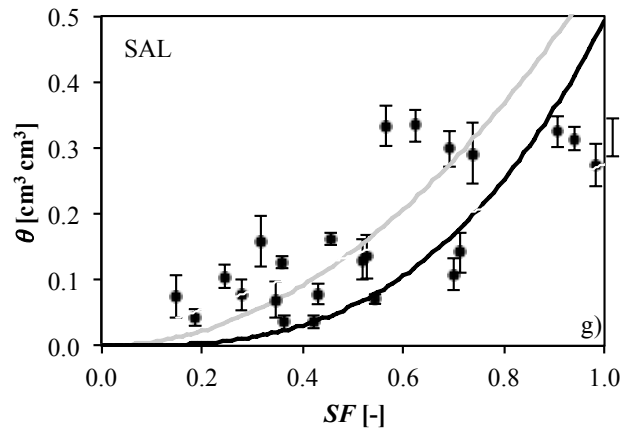
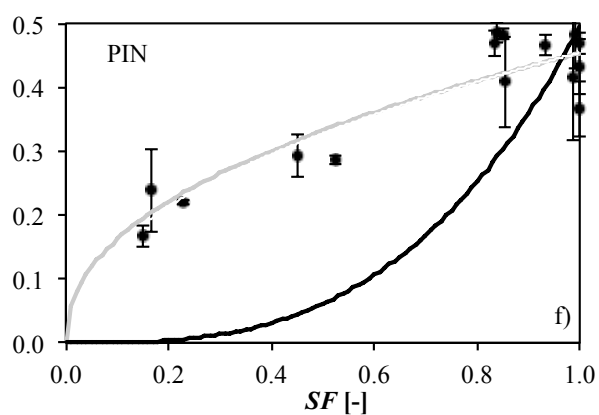
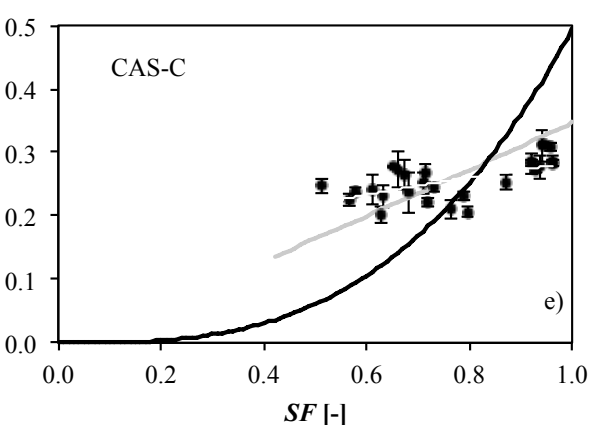
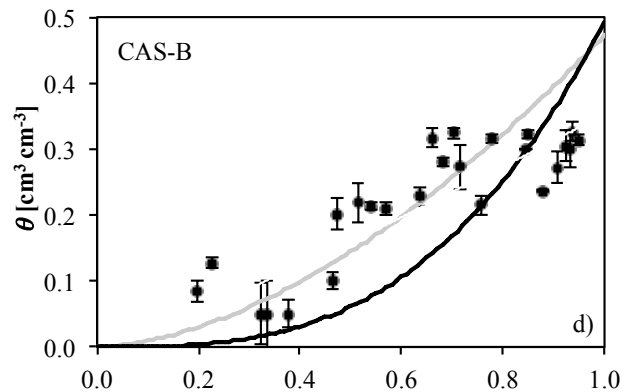
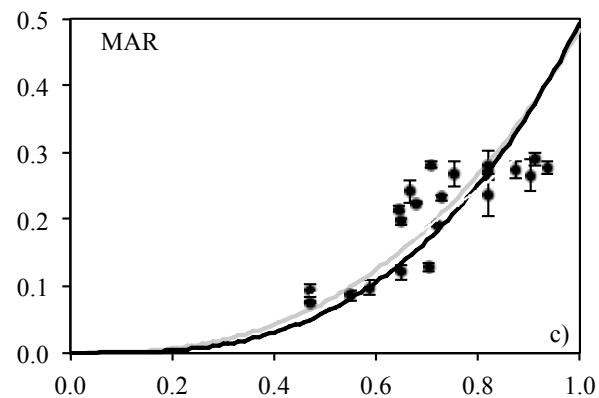
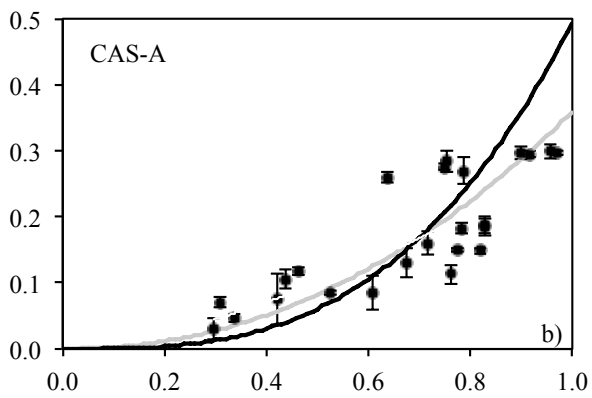
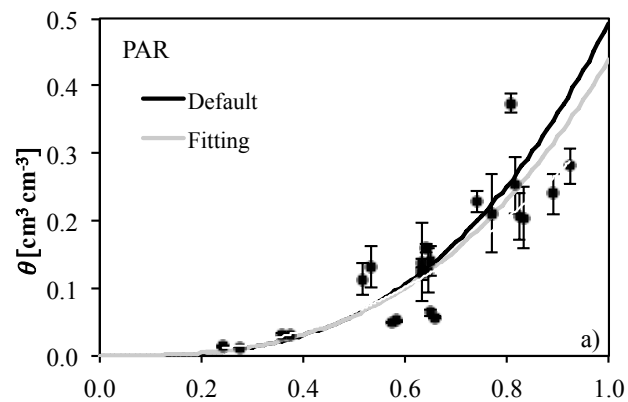


Fig6
[Click here to download Figure: fig6.pdf](#)

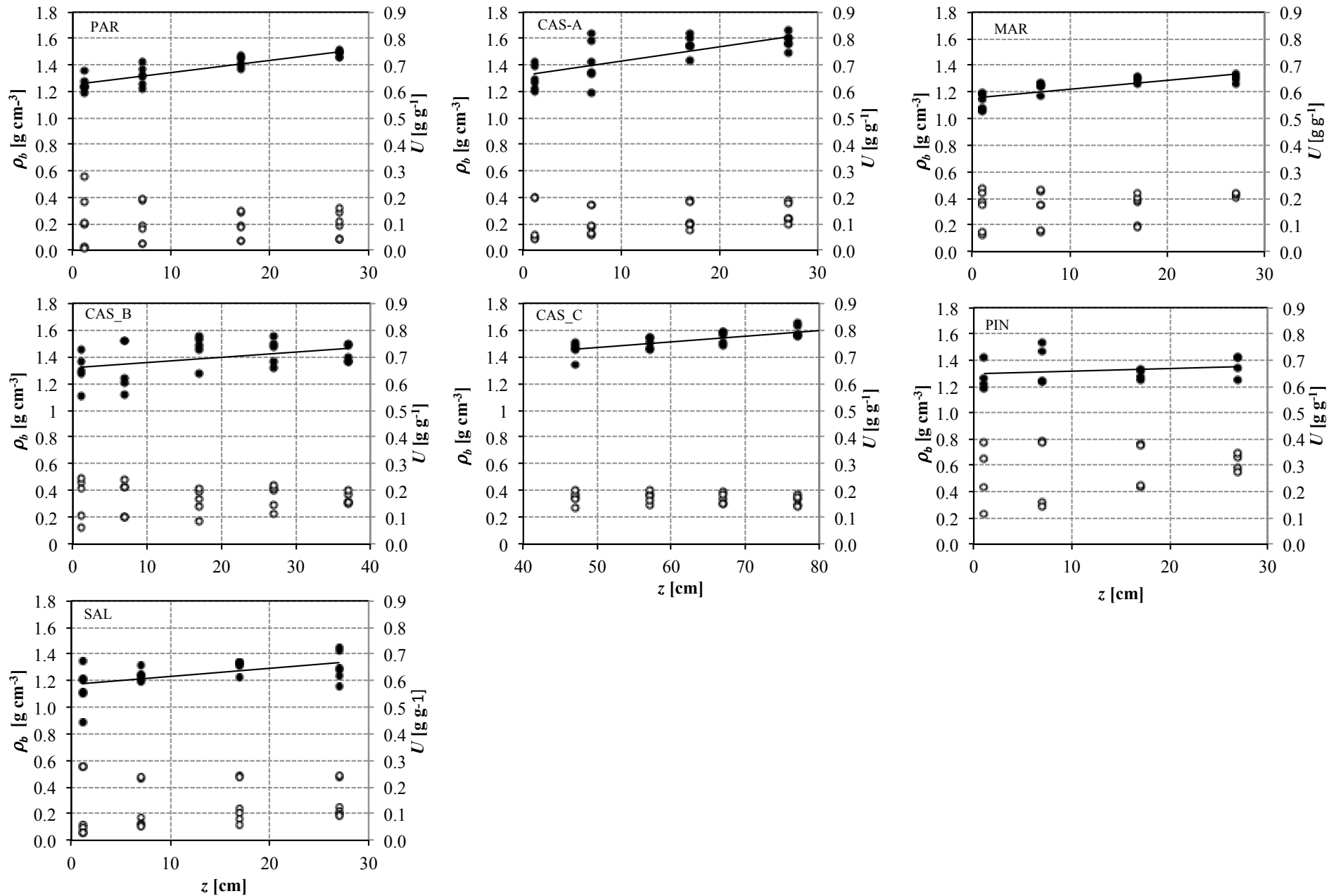


Fig7
[Click here to download Figure: fig7.pdf](#)

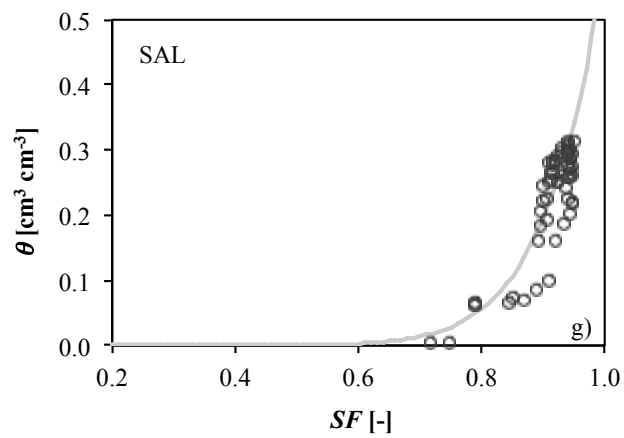
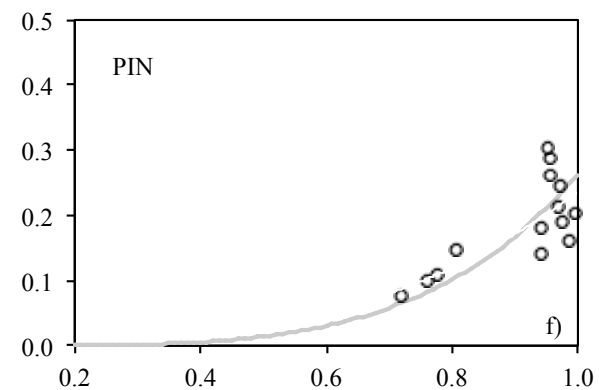
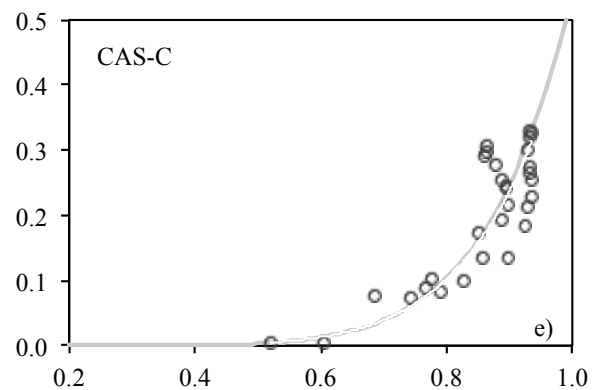
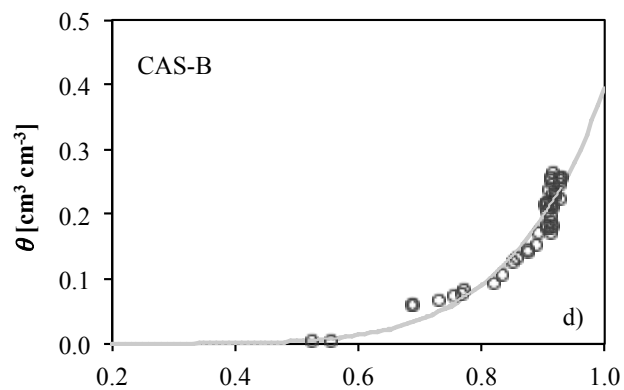
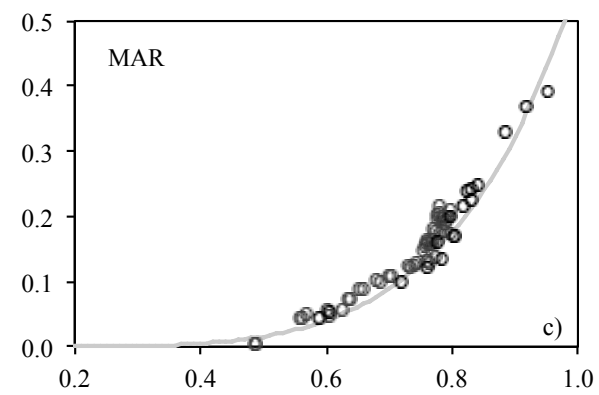
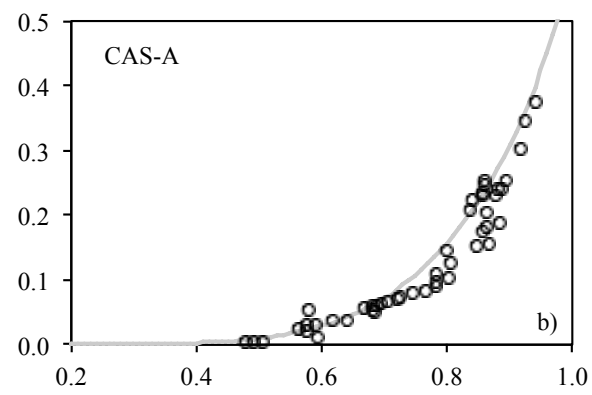
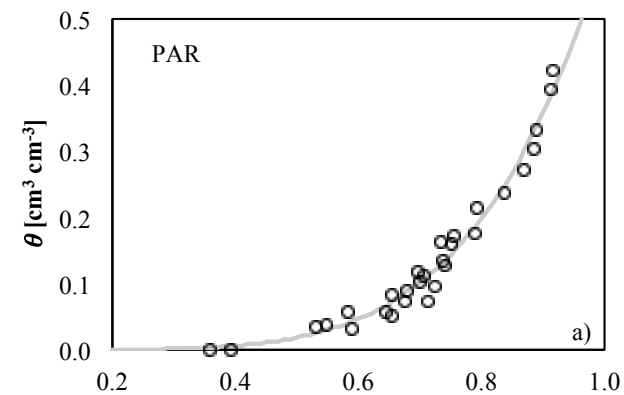


Fig8

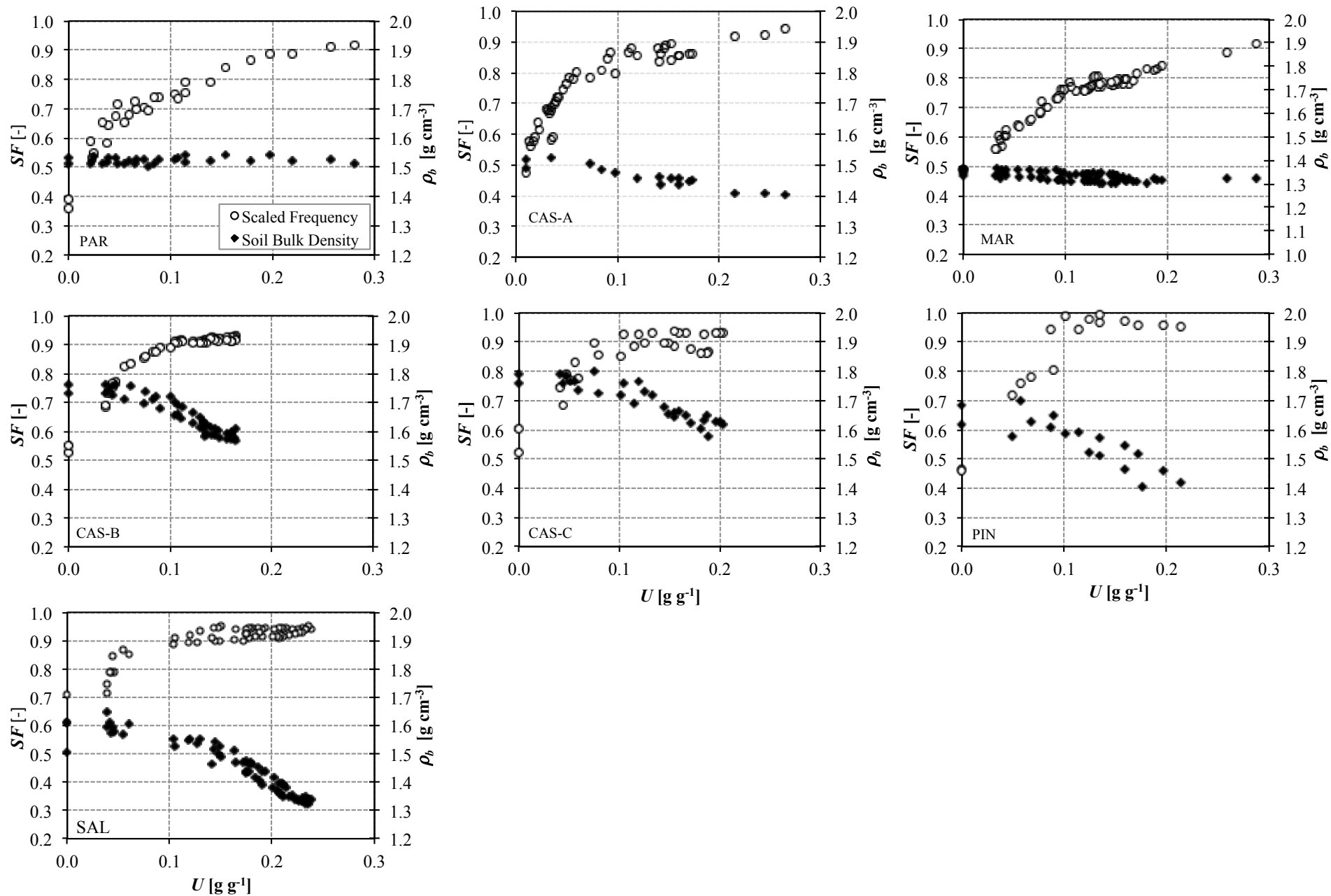
[Click here to download Figure: fig8.pdf](#)

Figure 1a,b - Schematic view of Diviner2000 probe; a) field calibration, b) laboratory calibration

Figure 2 - Map and localization of investigated sites (from Google Earth)

Figure 3a,i - Steps for collecting undisturbed soil monoliths

Figure 4 - Particle size distribution obtained on the investigated soils

Figure 5a-g - θ , SF data pairs measured in the field on different soils, in three experimental measurement campaigns. Error bars indicate the standard deviations of measured θ . Fitting regressions, as well as the default calibration equation are also shown

Figure 6a-g - Values of soil bulk density (black dots) and corresponding gravimetric water contents (white dots) measured on undisturbed soil samples (8.0 * 5.0 cm) as a function of soil depths

Figure 7a-g - Values θ (SF) measured on undisturbed soil monoliths and related fitting equation

Figure 8a-g - SF(U) (white dots) and ρ_b (U) (black dots) measured on undisturbed soil monoliths